Directional emission InP/GaInAsP square-resonator microlasers

Yong-Zhen Huang,* Kai-Jun Che, Yue-De Yang, Shi-Jiang Wang, Yun Du, and Zhong-Chao Fan

State Key Laboratory on Integrated Optoelectronics, Institute of Semiconductors, Chinese Academy of Sciences, Beijing 100083, China

**Corresponding author: yzhuang@semi.ac.cn*

Received June 6, 2008; revised July 29, 2008; accepted August 5, 2008; posted August 21, 2008 (Doc. ID 97152); published September 18, 2008

InP/GaInAsP square-resonator microlasers with an output waveguide connected to the midpoint of one side of the square are fabricated by standard photolithography and inductively-coupled-plasma etching technique. For a 20-μm-side square microlaser with a 2-μm-wide output waveguide, cw threshold current is 11 mA at room temperature, and the highest mode Q factor is 1.0×10^4 measured from the mode linewidth at the injection current of 10 mA. Multimode oscillation is observed with the lasing mode wavelength 1546 nm and the side-mode suppression ratio of 20 dB at the injection current of 15 mA.

OCIS codes: 140.2020, 140.3570, 140.3948, 230.3120, 230.5750, 250.5960.

Square optical resonators have attracted a great deal of interest for potential applications in microlasers and optical add–drop filters [1–12]. Square optical resonators can have long coupling lengths with input and output waveguides. However, an optical add–drop filter based on a perfect-square resonator can realize only a 25% drop in power owing to the standing-mode characteristics [1]. To realize a complete drop in power, as in traveling-wave mode resonator filters, coupled-square resonators [1] and deformed square resonators [2,3] were investigated as the square-resonator optical add–drop filters. Multimode resonances were observed in square-shaped μ cavities of fused silica [4,5], and single spatial-mode selection was realized in a layered square microcavity laser [6]. Mode field distribution and mode wavelength were derived for guided modes in a square resonator, which were in agreement very well with the numerical results of the finite-difference time-domain (FDTD) technique [7]. Furthermore, mode characteristics were numerically simulated for two-dimensional imperfect square microcavities [8] and three-dimensional microsquare resonators [9]. GaInAsP microsquare resonators supported by an InP pedestal were fabricated by the selectively etching technique, and obvious mode peaks were observed in the photoluminescence spectra of the resonators [10]. Very recently, high-Q lasing outputs were realized in square-shaped and deformed square-shaped organic–inorganic hybrid microdisks [11].

The inherent disadvantage of the total internal reflection and the isotropic emission of microdisks limits their directional emission for practical applications. To improve this deficiency, asymmetric points in the circular [12,13], quadrupolar [14], ellipse [15], and spiral-shaped [16] microdisk structures were applied to realize direction emission microlasers. In addition, highly directional output was achieved by coupling the microdisk resonator with a straight waveguide [17]. Recently, general designing rules of the deformation were discussed for realizing directional emission microcavity lasers [18]. For a square resonator with an output waveguide connected to the midpoint of one side, FDTD simulation indicated that the confined mode can have high Q factors, especially for the first-order transverse modes [19]. In this Letter, we report the fabrication and characteristics of cw electrically injected InP/GaInAsP square microlasers at room temperature.

The InP/GaInAsP laser wafer with the active region consising of seven quantum wells is grown by metal-organic chemical-vapor deposition on (001) InP substrate, where the thicknesses of the quantum wells and the barrier layers are 7 and 12 nm, respectively. The active region is sandwiched between 100-nm-thick GaInAsP cladding layers, and the upper layers are a 1.5-μm-thick p-InP and a p^+-InGaAs ohmic contact layer. The square lasers with a 2-μm-wide output waveguide connected to the midpoint of one side of the square are fabricated by the similar technique process of the triangle lasers [20]. Firstly, an 800 nm SiO_2 was deposited by plasma-enhanced chemical-vapor deposition on the as-grown InP/GaInAsP laser wafer as a hard mask for dry etching. Next, the patterns of the square resonator with a short output waveguide are transferred onto the SiO_2 layer using standard photolithography and inductively-coupled-plasma (ICP) etching techniques. The patterned SiO_2 hard masks define the square and output waveguide geometry for subsequent ICP process to etch InP and GaInAsP. The ICP etching depth is about 8 μm, which is overetched owing to a controlling problem. After the ICP etching, a chemical etching process is used to improve the smoothness of the side walls of the squares, and then the residual SiO_2 hard masks on the top of the squares are removed using a diluted HF solution. The scanning-electron-microscope image of a square resonator with an output waveguide after the ICP and the chemical etching processes is shown in Fig. 1, where the covering layer on the top of the square is the SiO_2 mask layer. The square pattern has slightly rounded vertices mainly owing to pattern distortion during photolithography and the chemical etching process. The length of the output waveguide is determined by the mask patterns instead of a cleaving across the output

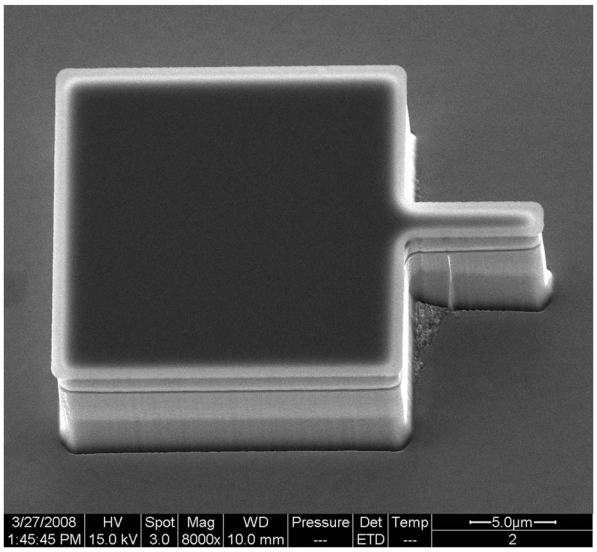

Fig. 1. Scanning-electron-microscope image of a square resonator after the ICP etching and wet chemically etching processes.

waveguide for the triangle lasers [20]. After that, a 400 nm SiO_2 insulating layer is deposited over the etched laser wafer, including the side walls of the square resonators. Then the SiO_2 insulating layer on the top of each square resonator is etched using another ICP etching process to open a contact window, and a Ti–Au p electrode is formed using a standard metal-deposition process over the laser wafer. Furthermore, a chemical etching process is used to etch the Ti–Au p electrode at the end of the output waveguide for realizing laser output. Finally, the laser wafer is lapped down to a thickness of about 100 μm, and an Au–Ge–Ni–Au metallization is used for the n-type contact on the other side of the InP substrate. The upper side of the fabricated square microlaser including the side walls of the square is covered with the SiO_2 insulating layer and the Ti–Au p electrode, except on the top of the square, where the SiO_2 insulating layer is etched by the ICP etching process for realizing current injection.

The output characteristics of a square laser with the side length $a=20$ μm were measured at room temperature without controlling temperature. The output power and the applied voltage versus the cw injection current are plotted as the solid and dashed curves in Fig. 2, respectively. The threshold current is 11 mA, and the highest output power is 0.07 mW as the injection current $I=36$ mA. From the applied voltages at the injection current $I=1$ and 50 mA, we estimate the series resistor to be 23 Ω. The rise of temperature, owing to the high series resistor, greatly limits the laser output power. At room temperature, the laser spectra are measured using an optical spectrum analyzer with a resolution of 0.1 nm. The lasing spectra of the square laser are plotted in Fig. 3 at $I=10$ and 15 mA. By fitting the resonance peaks marked by open squares in Fig. 3 with a Lorenztian function, we simple estimate the mode Q factor from the 3 dB bandwidth of each resonance peak. Mode Q factors of 3.1×10^3, 9.6×10^3, and 1.0×10^4

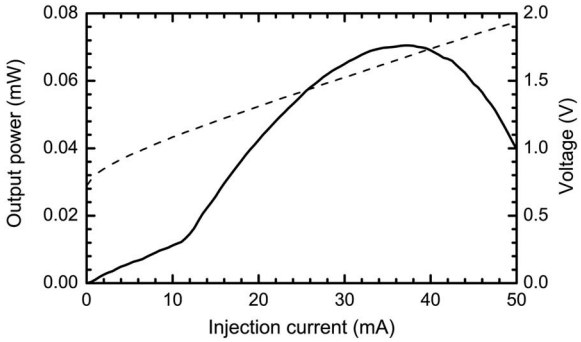

Fig. 2. Output power and applied voltage versus cw injected current for an InP/GaInAsP square laser with 20 μm side at room temperature.

are obtained for the mode at 1505.78, 1529.83, and 1546.07 nm from the laser spectrum at 10 mA. Multimode resonances are observed with the lasing wavelength of 1546.4 nm and the side-mode suppression ratio of 20 dB at $I=15$ mA.

In the square resonator, Fabry–Perot mode interval is $\delta\lambda_{FP}=\lambda^2/2an_g$ for the mode light ray near normal incident at the sides of the square, and the longitudinal mode interval for the whispering-gallery-type modes is $\delta\lambda=\lambda^2/2\sqrt{2}an_g$ [10], which is consistent with the normal modes at 45° ray's incident angle [4], where n_g is the group index of the square. We observed the mode interval of $\delta\lambda$ from photoluminescence spectrum of the disk-type square resonator supported by a pedestal with side length $a=7$ μm [10]. But the unpublished photoluminescence spectra of 15- and 20-μm-side square resonators exhibited much wider resonance peaks with the mode interval of $\delta\lambda_{FP}$, because the Fabry–Perot modes have higher output coupling efficiency than the whispering-gallery-type modes. We can expect that the laser spectra in Fig. 3 are influenced by the whispering-gallery-type modes and the Fabry–Perot modes. From the envelope of the resonance modes, we find several evident dips, with two of them at the wavelengths of 1513.60 and 1529.15 nm marked by the up arrows in Fig. 3. Matching the corresponding wavelength interval 15.55 nm to the Fabry–Perot mode interval $\delta\lambda_{FP}$, we have the mode group index $n_g=3.71$ and the longitudinal mode interval $\delta\lambda=11.0$ nm for

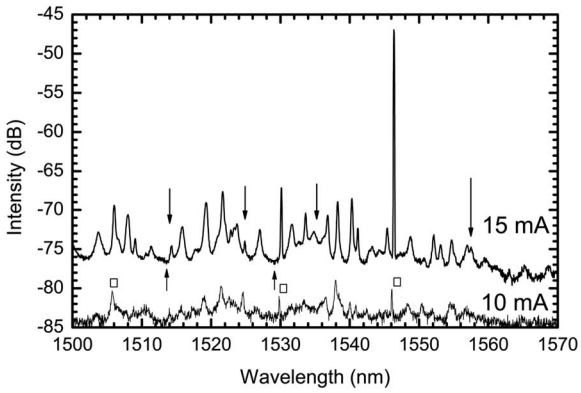

Fig. 3. Output spectra of the InP/GaInAsP square laser with 20 μm side at room temperature and cw injected current of 10 and 15 mA.

the whispering-gallery-type modes. The modes with the wavelength interval 11.0 nm relative to the lasing mode at 1546.4 nm are marked by the down arrows in Fig. 3, which should have the same transverse mode index as the lasing mode, but they are not strong resonance peaks. For another batch of square lasers with the highest lasing temperature about 200 K, we observed distinct peaks with wavelength intervals of 16 nm at room temperature and clear lasing modes with wavelength intervals of 10 nm at 200 K [21], which is much simpler than the laser spectrum in Fig. 3 at 15 mA.

Finally, to estimate the influence of the output waveguide on the mode Q factor, we numerically simulate a 20-μm-side square resonator with a 2-μm-wide output waveguide connected to the midpoint of one side of the square by 2D FDTD technique. In the simulation, the square resonator and output waveguide with refractive index 3.2 are confined by air instead of the SiO_2 insulating layer and the p-electrode layer, as in real devices. Two pulse-plane waves, centered at wavelength 1550 nm symmetric to the dashed line shown in the inset of Fig. 4, are added to excite symmetry modes relative to the middle line of the output waveguide. The time variation of a selected field component at some point inside the square is recorded as an FDTD output, and then the Padé approximation is used to transform the FDTD output from the time domain to frequency domain. The obtained intensity spectrum is plotted in Fig. 4, which shows that several modes have a Q factor larger than 10^4. So it is possible to realize that for low-threshold microlasers, even the width of the output waveguide is 2 μm. It should be noted that the laser spectra of Fig. 3 are contributed by the symmetric and antisymmetric modes. Furthermore, the mode interval obtained by FDTD simulation cannot be directly compared with the experimental results, because a constant refractive index is used in the numerical simulation.

In conclusion, we have fabricated InP/GaInAsP square lasers using conventional photolithography, the ICP etching technique, and the chemical etching process. The cw threshold current at room temperature is 11 mA for a 20-μm-side square laser. The lasing wavelength is 1546 nm, and the side-mode suppression ratio is 20 dB at 15 mA. We expect that the square microcavity laser is a potential light source for photonic integrated circuits and single-mode lasers.

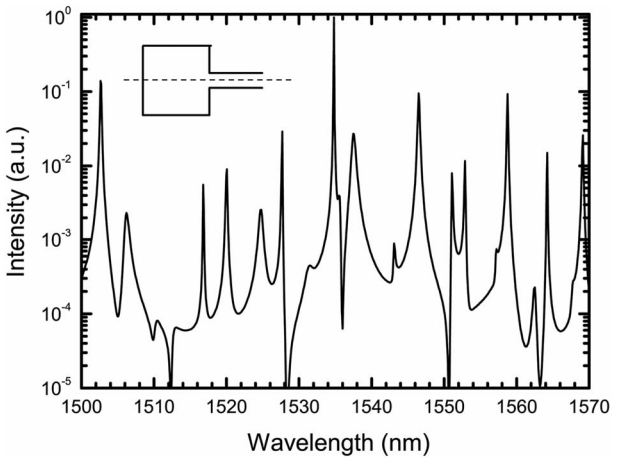

Fig. 4. Intensity spectrum obtained by the FDTD simulation for the symmetry modes relative to the middle line, shown as the dashed line in the inset, in the square with 20 μm sides and a 2-μm-wide output waveguide.

We gratefully acknowledge Jiao-Qing Pan for providing the laser wafer and financial support from National Natural Science Foundation of China (NNSFC) under grants 60777028 and 60723002, and the Major State Basic Research Program under grant 2006CB302804.

References

1. C. Manolatou, M. J. Khan, S. Fan, P. R. Villeneuve, H. A. Haus, and J. D. Joannopoulos, IEEE J. Quantum Electron. **35**, 1322 (1999).
2. C. Y. Fong and A. W. Poon, Opt. Express **11**, 2897 (2003).
3. Q. Chen, Y. D. Yang, and Y. Z. Huang, Opt. Lett. **32**, 967 (2007).
4. A. W. Poon, F. Courvoisier, and R. K. Chang, Opt. Lett. **26**, 632 (2001).
5. Y.-L. Pan and R. K. Chang, Appl. Phys. Lett. **82**, 487 (2003).
6. H. J. Moon, K. An, and J. H. Lee, Appl. Phys. Lett. **82**, 2963 (2003).
7. W. H. Guo, Y. Z. Huang, Q. Y. Lu, and L. J. Yu, IEEE J. Quantum Electron. **39**, 1563 (2003).
8. S. V. Boriskina, T. M. Benson, P. Sewell, and A. I. Nosich, IEEE J. Quantum Electron. **41**, 857 (2005).
9. Q. Chen, Y. Z. Huang, W. H. Guo, and L. J. Yu, IEEE J. Quantum Electron. **41**, 997 (2005).
10. Y. Z. Huang, Q. Chen, W. H. Guo, and L. J. Yu, IEEE Photonics Technol. Lett. **17**, 2589 (2005).
11. X. Wu, H. Li, L. Liu, and L. Xu, IEEE J. Quantum Electron. **44**, 75 (2008).
12. A. F. J. Levi, R. E. Slusher, S. L. McCall, J. L. Glass, S. J. Pearton, and R. A. Logan, Appl. Phys. Lett. **62**, 561 (1993).
13. Y. Chu, M. K. Chin, W. G. Bi, H. Q. Hou, C. W. Tu, and S. T. Ho, Appl. Phys. Lett. **65**, 3167 (1994).
14. C. Gmachl, F. Capasso, E. E. Narimanov, J. U. Nöckel, A. D. Stone, J. Faise, D. L. Sivco, and A. Y. Cho, Science **280**, 1556 (1998).
15. S. K. Kim, S. H. Kim, G. H. Kim, H. G. Park, D. J. Shin, and Y. H. Lee, Appl. Phys. Lett. **84**, 861 (2004).
16. G. D. Chern, H. E. Tureci, A. D. Stone, R. K. Chang, M. Kneissl, and N. M. Johnson, Appl. Phys. Lett. **83**, 1710 (2003).
17. S. J. Choi, K. Djordjev, S. J. Choi, and P. D. Dapkus, IEEE Photonics Technol. Lett. **15**, 1330 (2003).
18. S. V. Boriskina, T. M. Benson, P. D. Sewell, and A. I. Nosich, IEEE J. Sel. Top. Quantum Electron. **12**, 1175 (2006).
19. W. Zhao and Y. Z. Huang, Chin. Opt. Lett. **5**, 463 (2007).
20. Y. Z. Huang, Y. H. Hu, Q. Chen, S. J. Wang, Y. Du, and Z. C. Fan, IEEE Photonics Technol. Lett. **19**, 963 (2007).
21. Y. Z. Huang, S. J. Wang, K. J. Che, Y. H. Hu, Y. Du, and L. J. Yu, in *Proceedings of 10th International Conference on Transparent Optical Networks*, M. Marciniak, ed. (IEEE, 2008), Vol. 4, p. 238.